SYNOVIAL FLUID PROFILE DICTATES NANOPARTICLE UPTAKE INTO CARTILAGE- IMPLICATIONS OF THE PROTEIN CORONA FOR NOVEL ARTHRITIS TREATMENTS

Ula von Mentzer[1], Tilia Selldén[1], Loise Råberg[1], Gizem Erensoy[1], Anna-Karin Hultgård-Ekwall[2,3], Alexandra Stubelius[1,]*

[1]*Division of Chemical Biology, Department of Biology and Biological Engineering, Chalmers University of Technology, Gothenburg, Sweden.*

[2]*The Rheumatology Clinic, Sahlgrenska University Hospital, Gothenburg, Sweden.*

[3]*Department of Rheumatology and Inflammation Research, Institute of Medicine, Sahlgrenska Academy of University of Gothenburg, Gothenburg, Sweden.*

*Corresponding author: Alexandra Stubelius, Alexandra.stubelius@chalmers.se

Postal address: Kemivägen 10, 41296 Gothenburg, Sweden

Keywords: Drug delivery; cartilage, synovial fluid, PAMAM, osteoarthritis, rheumatoid arthritis, protein corona / adsorption

ABSTRACT

Intra-articular drug delivery strategies aiming to deliver drugs in diseases affected by cartilage-related issues are using electrostatic interactions to penetrate the dense cartilage matrix. This enables delivery of sufficient drug concentrations to the chondrocytes to mediate the desired therapeutic effect. As it is well known that size and charge of nanoparticles affects its interactions with the surrounding biological fluids, where proteins adsorb to the NP surface, resulting in a protein corona. There are, however, no studies investigating how the formed protein coronas affect cartilage uptake and subsequent cellular uptake, nor how they affect other cells present in the synovium of such diseases. Here, we explore the differences between the protein coronas that form when NP are incubated in synovial fluid from osteoarthritic and rheumatoid arthritis patients and compare this to results obtained using fetal calf serum (FCS), as guide for researchers working on joint drug delivery. We demonstrate that the protein corona indeed affects the uptake into cartilage, where there are major differences between the model proteins in fetal calf serum, as compared to synovial fluid from rheumatoid arthritis patients as well as osteoarthritis patients. The data suggests that when developing drug delivery vehicles for joint diseases that leverages electrostatic interactions and size, the interactions with proteins in the biological milieu is highly relevant to consider.

1. INTRODUCTION

Diseases affecting the joints such as osteoarthritis (OA) are on the rise due to our increasingly aging and overweight population[1]. The world health organization estimate that 9,6 of men and 18% of women aged 60 and above have symptomatic OA, yet there are no disease-modifying therapies available to slow down disease progression. A major issue for drug delivery in OA has been an inability to reach the chondrocytes deeply embedded in the cartilage[1, 2]. The cartilage extracellular matrix is a dense, avascular, and aneural network of large and highly negatively charged protein macromolecules. Intra-articular drug delivery approaches are now leveraging these unique ECM characteristics, including designing nanosized approaches that via electrostatic attractions penetrate the anionic ECM[2, 3]. However, drug delivery vehicles entering the body are immediately coated with host-derived biological

components such as proteins, carbohydrates and lipids[4]. Here, the physicochemical attributes of the nanoparticles will affect the formation of the protein corona[5-8]. These components alter the size and surface composition of the particles and provide them with a biological identity distinct for their synthetic identity. This protein corona formation has been extensively studied in drug delivery vehicles administered to the blood, yet for drug delivery vehicles targeting the cartilage, no studies exist so far that examines the nature of the synovial fluid on the protein corona composition. The importance of selecting a proper biological milieu for protein corona analysis in vitro was demonstrated in studies comparing human plasma versus human serum, where there was a profound difference in both protein corona composition and nanoparticle fate, demonstrating the importance of selecting the proper environment to mimic in vivo settings[9]. Factors that have been proven to highly affect the corona include size and charge, which are the main components are leveraged for passive intra-articular drug delivery vehicles into the cartilage[3]. The aim of this study was to examine the nature of the formed protein corona in synovial fluid from OA patients compared to synovial fluid from rheumatoid arthritis (RA) patients, as well as to the more frequently used fetal bovine serum (FBS), in order to understand how this affects the cartilage uptake for therapeutic translation.

2. Results and Discussion

2.1 2.1 Material Composition and Characterization

The studies below are based on polyamidoamine (PAMAM) dendrimeric nanoparticles, as they are easily manipulated and can be tuned both for charge and size by facile surface conjugation. Dendrimeric structure of the nanoparticles result in multiple surface groups giving rise to positively charged material whose surface is decorated with amino groups. The highly cationic nature of these nanoparticles has paved the way for their use in drug delivery due to their electrostatic attraction to negatively charged materials such as nucleic acids and extracellular matrix proteins. However, since strong electrostatic interactions are not always desirable due to increased cytotoxicity, protein adsorption or decreased stability of the system, utilization of various polymers such as polyethene glycol and others has been successfully explored to tune nanoparticle physicochemical properties[10, 11]. In particular, PEGylation has been an attractive strategy as PEG offers good stability, hydrophilicity, and its biocompatibility

with immune system and biological protein interactions has been extensively remarked[11, 12]. Here we have designed three types of PAMAM-based particles that surface chemistry, size, and charge. To have a variety of different surface chemistries, two mPEGs of different molecular weights, 350 or 5000 were used for the PEGylation reaction. No PEG was used for one group of samples to yield a more positive charge of the particles. PEGylation was performed according to Ma et al.[13], and verified by 1H-NMR (Supplementary Figure S1). To retain the positive PAMAM profile, we limited PEGylation to 2% mPEG conjugation. Particles were also labelled with fluorescein isothiocyanate, FITC that further contributed to the changes on the nanoparticle surface (Supplementary Figure S1.). Nanoparticle size was assessed using electron microscopy imaging and dynamic light scattering (Figure 1, A and B, respectively) was used to assess nanoparticle hydrodynamic diameter, FITC signal, as well as the zeta potential in physiological pH conditions (Figure 1 B,C,D).

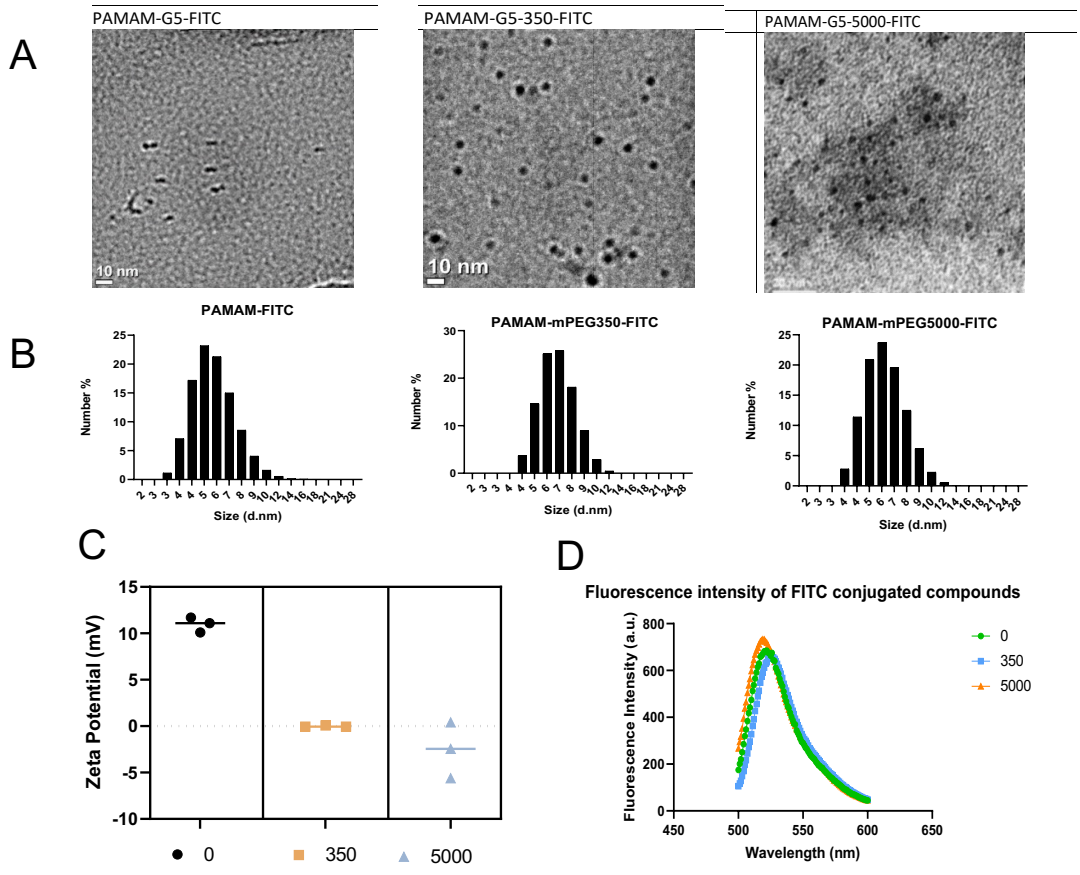

Figure 1. PAMAM-mPEG-FITC nanoparticle characterization. The size of the nanoparticles was assessed with TEM (A) in a 15uM PBS suspension at pH=6. Hydrodynamic diameter of the particles was measured in 30uM, neutral pH environment and the values were extracted based on the size

distribution by volume. PAMAM-FITC nanoparticles measured 5.720 nm ±1.442 S.D., PAMAM-mPEG-350-FITC - 5.980 nm ±1.494 S.D, and PAMAM-mPEG-5000-FITC – 7.776 nm ±2.432 (B). To practically assess the effect of FITC conjugation, FITC signal was measured and quantified λex 483-14 nm/ λem 530-30 nm. The concentrations to achieve a similar FITC intensity profile among all the samples are: 1.5uM PAMAM-mPEG350-FITC, 3uM PAMAM-FITC, and 30uM PAMAM-mPEG5000-FITC (C). Zeta potential was quantified using DLS resulted in 11 mV for PAMAM-FITC ±0.81 S.D., 0 mV ±0.07 S.D. for PAMAM-mPEG-350-FITC, and -2.819 mV ±3.01 S.D. for PAMAM-mPEG-5000-FITC (D).

TEM micrographs depict the dispersed nanoparticles at the expected sizes (theoretical size PAMAM G5= 5.4nm). The PAMAM nanoparticle solution pH was adjusted to 6 to protonate the tertiary PAMAM groups and to avoid aggregation of the sample due to water evaporation.

Similar size observations were recorded by DLS in hydrodynamic diameter evaluation. Although the values measured by DLS (Figure 1B) were slightly higher than those acquired by imaging due to the differences in measuring techniques.

As PAMAM particles were not only PEGylated but also labelled with a fluorescent tag, FITC, the variation in fluorescence signal was assessed among the three synthesized particles. At the same concentration (30uM), PAMAM-mPEG350-FITC displayed the highest green fluorescence intensity, while PAMAM-mPEG5000-FITC resulted in the lowest signal of fluorescence. It is likely that the latter sample labelling efficiency was affected by the long, free moving mPEG5000 chains in the solution which at any given point may mask the otherwise exposed amino surface groups. Figure 1C illustrates the optimized concentrations of each of the samples to account for the differences in FITC conjugation efficiency. Interestingly, PAMAM-FITC fluorescence signal was inferior to the PEGylated 350 sample. A trend in nanoparticle zeta potential (Figure D) agrees with the size measurement observations, where the particle change in size is correlated with the decreasing charge trend. As expected, the highest positive charge was observed in particles containing no PEG, as it was only the FITC molecules occupying the nanoparticles' surface. In addition, PAMAM-mPEG350-FITC particles were

characterized by a neutral charge, while PAMAM- mPEG5000-FITC sample displayed the least constant, negative zeta potential value.

2.2 Cartilage Uptake studies of protein-corona coated NPs

Given that the nature of cartilage tissue is characterized by the negative charge due to the presence of carboxyl and sulphate groups on glycosaminoglycans present in the tissue matrix, we wanted to investigate how the differences in our nanoparticles would affect the cartilage uptake in a protein-abundant environment. The effect of protein adsorption to nanoparticles and their influence on the particle efficacy are rarely addressed in nanoparticle characterization studies. Here we assessed the cartilage uptake of nanoparticles in presence of inflammatory, protein rich synovial fluids from rheumatoid arthritis and osteoarthritis patients (Fig. 2).

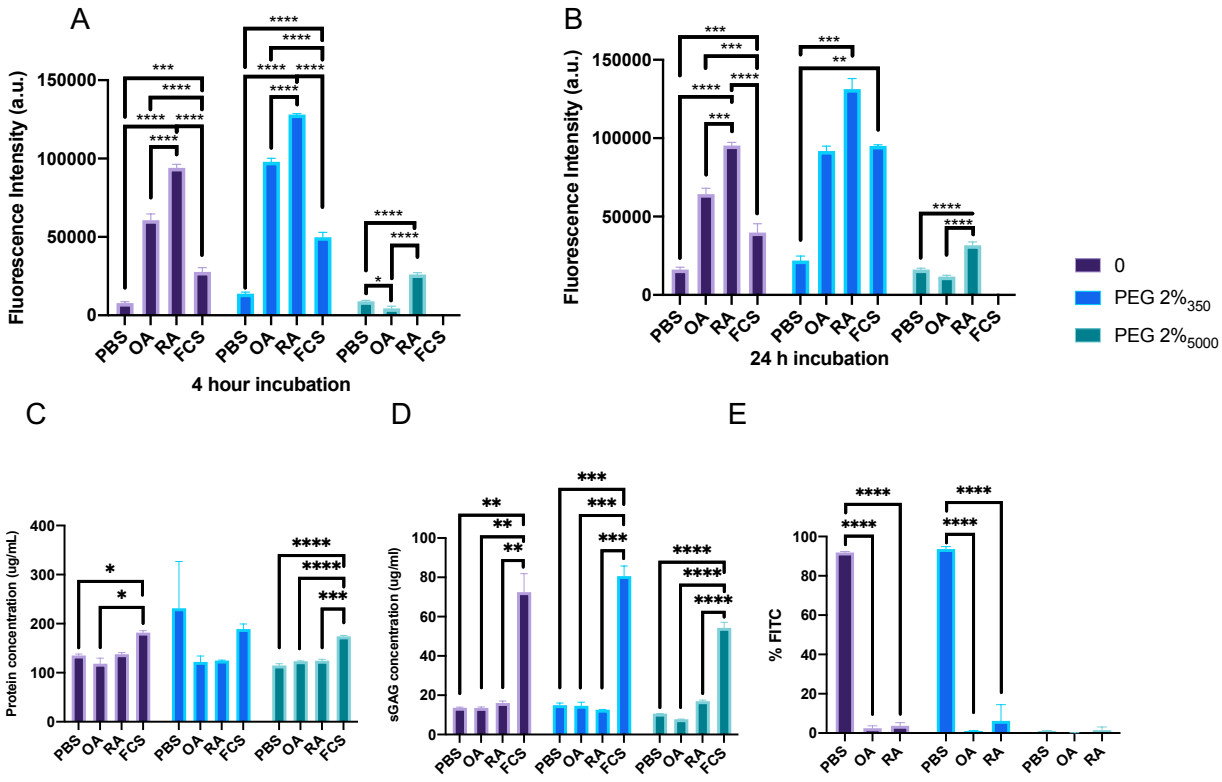

Figure 2. Investigation of PAMAM-mPEG$_x$-FITC nanoparticle uptake to the cartilage tissue explants in presence of patient synovial fluids. 30uM of each nanoparticle suspension was exposed to four different protein abundance conditions – no protein = PBS, pooled OA patient synovial fluid (2f/2m), pooled RA patient synovial fluid (4f/1m), or fetal calf serum (FCS). After nanoparticle-protein coronas

were isolated, samples were incubated for 4h (A) or 24h (B) with cartilage explants that were extracted from adult pigs and the FITC intensity was measured to quantify the particle uptake. The protein concentration in the supernatant post-explant incubation was quantified using BCA assay (C) and a further DMMB assay was performed to assess cartilage matrix protein (sGAG) concentration (D). Additionally, the cellular uptake of nanoparticle-corona complexes were assessed using a chondrocyte (Tc28a2) cell line and expressed as a percentage (E).

The particles were incubated with synovial fluid or fetal calf serum (FCS) as control for one hour and then subjected to cartilage explant uptake studies for either 4 or 24 hours. After indicated incubations, the FITC signal was measured in the surrounding media, where a decreased FITC signal is assumed to be due to uptake into the cartilage tissue. An overall high FITC fluorescence intensity signal was detected when comparing naked particles to particles with a protein corona after both 4h and 24h (Figure 2A and 2B), suggesting that the protein corona does affect cartilage uptake. Due to the difference in fluorescence intensity, we choose to compare the results within particles, and not compare the different particle sizes. The commonly used FCS as a supplement in cell culture studies was found to have an influence on cartilage uptake when compared to no protein control, however the largest impact is seen after the NPs are incubated with synovial fluid samples. These results are highly interesting, as the protein concentration from these studies indicate no difference in protein amounts (Fig. 2C), but instead is believed to originate from the nature of the proteins in the corona. Additionally, the protein quantification revealed similar protein concentration among the different conditions and different nanoparticles. To assess whether the synovial fluids and their inflammatory profiles had any influence on the explant integrity, we quantified the sulphated glycosaminoglycan concentration in the post-experimental cartilage explant supernatants (Fig. 2D). FCS condition resulted in the highest quantity of sGAGs, which was not related to the potential presence of sGAGs in the FCS, as unprocessed FCS did not elicit a signal (results not shown). The differences in the functions of the proteins that form the coronas could affect how cells interact with the NPs, which prompted us to assessed the uptake of the NPs by chondrocytes[1]. After 4 hours, the naked NPs were still eliciting a strong FITC expression, either indicating that the corona-coated particles already had been processed at this timepoint, or that they are taken up to a less extent as compared to naked NPs (Fig. 2E).

2.3 Characterization of protein corona-coated NPs

As we have confirmed the differences based on nanoparticle surface chemistry and protein-abundant conditions, we sought to investigate the individual differences in hard-corona protein profile for each type of our nanoparticle. The particle-protein corona was prepared the same as for the experiments above. The sample pellets were then snap-frozen with liquid nitrogen and submitted to Gothenburg Proteomics Core Facility for the LC-MS/MS analysis. The total number of proteins identified for RA, OA, and FCS are 2543, 2332, and 686, respectively. FCS condition resulted in the biggest percentage of protein on PAMAM-mPEG350-FITC particles (95.5%), while PAMAM-FITC and PAMAM-mPEG5000-FITC particles both attracted ~88% of total proteins identified in FCS sample. Osteoarthritic synovial fluid showed an opposite trend, where PAMAM-mPEG350-FITC attracted the least amount of protein (75.9%), while PAMAM-FITC showed 82.3% and PAMAM-mPEG5000-FITC demonstrated highest adsorption of the total identified protein (86.8%). Finally, PAMAM-FITC attracted the most proteins in RA condition (89.6%), while PAMAM-mPEG350-FITC and PAMAM-mPEG5000-FITC contained 85.3% and 83.8% respectively. The protein abundances were normalized and top 25 proteins with highest abundance for each condition per nanoparticle are depicted in Figure 3.

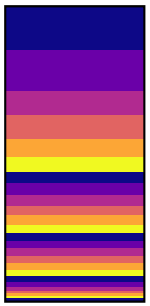

RA-0

- Fibrinogen alpha chain
- Albumin
- Histone H3.1
- Inter-alpha-trypsin inhibitor heavy chain H2
- Trypsinogen isoform X1
- Histone H4
- Apolipoprotein A-I
- Complement C3
- Apolipoprotein B-100
- Apolipoprotein C-III
- Fibrinogen gamma chain
- Inter-alpha-trypsin inhibitor heavy chain H1
- Immunoglobulin heavy constant mu
- Proteoglycan 4
- Fibronectin
- Fibrinogen beta chain
- Vitronectin
- Clusterin
- Myeloperoxidase
- Apolipoprotein E
- Immunoglobulin heavy constant gamma 4
- Immunoglobulin J chain
- Complement component C9
- Immunoglobulin heavy constant alpha 1
- Cathepsin G

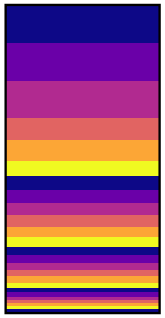

RA-350

- Albumin
- Inter-alpha-trypsin inhibitor heavy chain H2
- Fibrinogen alpha chain
- Histone H3.1
- Inter-alpha-trypsin inhibitor heavy chain H1
- Fibronectin
- Trypsinogen isoform X1
- Histone H4
- Complement C3
- Apolipoprotein B-100
- Vitronectin
- Fibrinogen gamma chain
- Apolipoprotein A-I
- Apolipoprotein E
- Apolipoprotein C-III
- Immunoglobulin heavy constant mu
- Clusterin
- Fibrinogen beta chain
- Complement component C9
- Proteoglycan 4
- Immunoglobulin J chain
- Immunoglobulin heavy constant gamma 4
- Immunoglobulin heavy constant alpha 1
- C4b-binding protein alpha chain
- Inter-alpha-trypsin inhibitor heavy chain H3

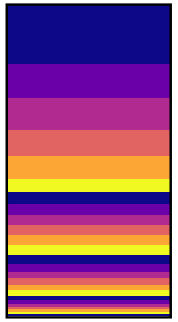

RA-5000

- Fibrinogen alpha chain
- Albumin
- Histone H3.1
- Trypsinogen isoform X1
- Histone H4
- Fibronectin
- Fibrinogen gamma chain
- Apolipoprotein A-I
- Apolipoprotein B-100
- Complement C3
- Proteoglycan 4
- Apolipoprotein C-III
- Fibrinogen beta chain
- Myeloperoxidase
- Immunoglobulin heavy constant mu
- Vitronectin
- Clusterin
- Apolipoprotein E
- Immunoglobulin heavy constant gamma 4
- Transmembrane protein 132A
- Cathepsin G
- Immunoglobulin heavy constant alpha 1
- Vimentin
- Immunoglobulin J chain
- Neuroblast differentiation-associated protein AHNAK

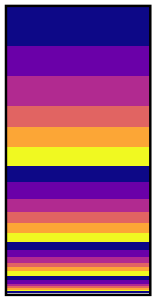

OA-0

- Fibrinogen alpha chain
- Fibronectin
- Trypsinogen isoform X1
- Albumin
- Proteoglycan 4
- Complement C3
- Inter-alpha-trypsin inhibitor heavy chain H2
- Apolipoprotein B-100
- Apolipoprotein C-III
- Apolipoprotein A-I
- Clusterin
- Fibrinogen beta chain
- Vitronectin
- Fibrinogen gamma chain
- Apolipoprotein E
- Hemoglobin subunit alpha
- Inter-alpha-trypsin inhibitor heavy chain H1
- Histone H4
- Histone H3.1
- Apolipoprotein A-IV
- Alpha-2-HS-glycoprotein
- Prothrombin
- Gelsolin
- Alpha-1-antitrypsin
- Complement component C9

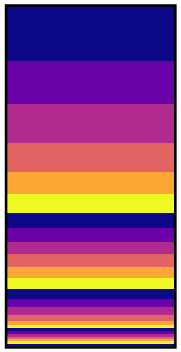

OA-350

- Albumin
- Fibrinogen alpha chain
- Inter-alpha-trypsin inhibitor heavy chain H2
- Fibronectin
- Complement C3
- Trypsinogen isoform X1
- Proteoglycan 4
- Apolipoprotein B-100
- Inter-alpha-trypsin inhibitor heavy chain H1
- Apolipoprotein C-III
- Vitronectin
- Fibrinogen gamma chain
- Clusterin
- Fibrinogen beta chain
- Apolipoprotein A-I
- Apolipoprotein E
- Histone H3.1
- Cartilage acidic protein 1
- Apolipoprotein A-IV
- Complement component C9
- Hemoglobin subunit alpha
- Complement C1s subcomponent
- Alpha-2-HS-glycoprotein
- Transthyretin
- Cartilage oligomeric matrix protein

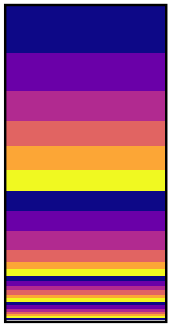

OA-5000

- Albumin
- Trypsinogen isoform X1
- Apolipoprotein C-III
- Apolipoprotein B-100
- Proteoglycan 4
- Apolipoprotein A-I
- Fibronectin
- Complement C3
- Clusterin
- Fibrinogen alpha chain
- Apolipoprotein E
- Vitronectin
- Apolipoprotein A-IV
- Fibrinogen beta chain
- Histone H3.1
- Alpha-2-HS-glycoprotein
- Gelsolin
- Complement component C9
- Hemoglobin subunit alpha
- Histone H4
- Fibrinogen gamma chain
- Inter-alpha-trypsin inhibitor heavy chain H4
- Inter-alpha-trypsin inhibitor heavy chain H2
- Band 3 anion transport protein
- Myeloperoxidase

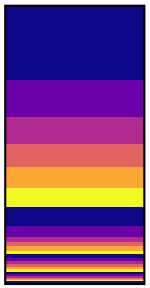

FCS-0

- Alpha-2-HS-glycoprotein
- Serum albumin
- Apolipoprotein A-I
- Apolipoprotein A-II
- Hemoglobin subunit alpha
- Alpha-1-antiproteinase
- Hemoglobin fetal subunit beta
- Alpha-fetoprotein
- Fetuin-B
- Inter-alpha-trypsin inhibitor heavy chain H3
- Complement C3
- Prothrombin
- Inter-alpha-trypsin inhibitor heavy chain H4
- Alpha-1B-glycoprotein
- Gelsolin
- Alpha-2-macroglobulin
- Pigment epithelium-derived factor
- Aggrecan core protein
- Plasminogen
- Complement factor B=9913 GN=CFB
- Galectin-3-binding protein
- Actin, cytoplasmic 1
- Inter-alpha-trypsin inhibitor heavy chain H1
- Apolipoprotein E
- Lumican

FCS-350

- Alpha-2-HS-glycoprotein
- Serum albumin
- Hemoglobin subunit alpha
- Inter-alpha-trypsin inhibitor heavy cl
- Alpha-1-antiproteinase
- Hemoglobin fetal subunit beta
- Alpha-fetoprotein
- Complement C3
- Inter-alpha-trypsin inhibitor heavy cl
- Gelsolin
- Pigment epithelium-derived factor
- Apolipoprotein A-I
- Inter-alpha-trypsin inhibitor heavy cl
- Alpha-2-macroglobulin
- Fetuin-B
- Alpha-1B-glycoprotein
- Complement factor B
- Plasminogen
- Apolipoprotein E
- Prothrombin
- Thrombospondin-1
- Protein AMBP
- Thyrine-binding globulin
- Fibrinogen beta chain
- Actin, cytoplasmic 1

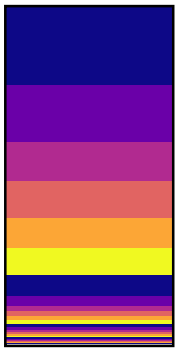

FCS-5000

- Alpha-2-HS-glycoprotein
- Serum albumin
- Apolipoprotein A-II
- Apolipoprotein A-I
- Hemoglobin fetal subunit beta
- Alpha-1-antiproteinase
- Hemoglobin subunit alpha
- Alpha-fetoprotein
- Alpha-2-macroglobulin
- Fetuin-B
- Inter-alpha-trypsin inhibitor heavy chain H4
- Complement C3
- Alpha-1B-glycoprotein
- Inter-alpha-trypsin inhibitor heavy chain
- Gelsolin
- Apolipoprotein C-III
- Pigment epithelium-derived factor
- Complement factor B
- Plasminogen
- Alpha-2-antiplasmin
- Apolipoprotein E
- Keratin, type I cytoskeletal 10
- Actin, cytoplasmic 1
- Inter-alpha-trypsin inhibitor heavy chain H1
- Vitamin D-binding protein

Figure 3. Individual protein-corona composition consisting of top 25 proteins of highest abundance. The normalized abundances were converted to percentages to signify their value in the top 25. Trypsin associated proteins may arise due to data processing with trypsin and protease inhibitor interactions during the sample preparation. Please note that FCS samples were analyzed against bovine animal database, while RA and OA samples were compared with human database.

High abundance proteins including albumin, complement, and certain apolipoproteins seemed to be universal for both RA and OA, some condition distinct factors were identified. FCS samples contained proteins such as Galectin-3-binding protein and lumican which proved to be unique from the rest of the samples. RA samples proved to be rich in immunoglobulins, while OA synovial fluid exhibited unique expression of proteins such as cartilage acidic protein 1 and cartilage oligomeric matrix protein (COMP), although the corona profiles between these two conditions overall contained a lot of similarity. It is important to note that due to inflammatory nature of rheumatoid arthritis, more immune system associated proteins were identified in RA samples.

2.5 Conclusion

In conclusion, these data demonstrate that the nature of the biological environment that a designed drug delivery vehicle will interact with is important to take into consideration[14]. This is in line with previous studies on serum and plasma nanoparticle interactions, demonstrating a major impact despite being from the same blood stream. Protein adsorption is enhanced by hydrogen bonds, Van der Waals interaction and not the least electrostatic interactions. Considering the importance of utilizing electrostatic interactions to enhance drug delivery to penetrate the dense cartilage matrix for joint diseases such as OA, this study contributes to the research field by providing solid evidence that the protein corona and the nature of synovial fluid needs to be taken into consideration when designing these drug delivery vehicles.

3. Experimental Section

3.1 Materials and Reagents

Ethylenediamine core amino-terminated PAMAM dendrimer Generation 5 manufactured by Dendritech (CAS: 163442-68-0), methoxypolyethylene glycols (mPEG) 350 and 5000 (CAS:9004-74-4), 4-(Dimethylamino)pyridine (DMAP) ≥99% (CAS:1122-58-3), PMA (CAS:16561-29-8), 4-nitrophenyl chloroformate (4-NPC) 97% (7693-46-1) manufactured by Acros Organics, fluorescein isothiocyanate isomer I (CAS:3326-32-7), resazurin sodium salt (CAS: 62758-13-8), and chondroitin 4-sulfate sodium salt from bovine trachea (39455-18-0) were all purchased from Sigma-Aldrich (Munich, Germany).

DPBS (1X) without calcium and magnesium (manufactured by Gibo), dichloromethane (CAS:75-09-2), dimethyl sulfoxide (CAS: 67-68-5), deuterium oxide (CAS:7789-20-0) manufactured by Acros Organics, DMEM (Dulbecco's Modified Eagle's Medium), RPMI 1640 (Roswell Park Memorial Institute), fetal bovine serum (FBS), GlutaMAX by Gibco, and Pierce BCA protein assay kit were all purchased from Fisher Scientific (Waltham, USA).

3.2 Material Synthesis

3.2.1 PAMAM PEGylation

First, mPEG 350 or 5000, 4-NPC, and DMAP were combined using a molar ratio of 1: 1.5: 1.1, respectively and dissolved using dropwise addition of DCM. The reaction was stirred for 24 hours under nitrogen flow at room temperature. To obtain the product, most of the solvent was removed using rotary evaporator, while the product was precipitated over the excess chilled diethyl ether, collected using vacuum filtration and dried. The product of activated mPEG was purified by recrystallization using chloroform and diethyl ether, 10:1.

PAMAM G5 solvent was switched from methanol to deionized water. 1.585mM of PAMAM solution was diluted 1:10 using $NaHCO_3$ and pH value was adjusted to 8.0±0.08. mPEG350 and mPEG5000 were solubilized in DMSO while in 0% PEG condition, no mPEG was added. PEGylation was executed combining these solutions in a stochiometric ratio of 1:3 for PAMAM and (no) mPEG respectively. Mixtures were vortexed, covered and incubated overnight while shaking at room temperature. Samples were then dialyzed against deionized water using Spectra/Por 3 Regenerated Cellulose 6-8kD MWCO

tubing to remove DMSO and unreacted reagents. Synthesized compounds were lyophilized and stored in the fridge until further use.

3.2.1.1 Nuclear magnetic resonance (NMR)

^{1}H NMR spectra of the compounds were recorded with Agilent VnmrS spectrometer at 400 MHz. Samples were solubilized in D2O unless otherwise stated. Data was analyzed using MestReNova version 14.1.1.

3.2.2 FITC conjugation

PEGylated PAMAM compounds (0%, 2% 350 and 2% 5000) were dissolved in PBS (pH=7.4) at 5mg/mL and were allowed to react with fluorescein isothiocyanate isomer I (FITC) which was dissolved in acetone at 1:5 molar ratio respectively. The reaction was carried on in the dark for 12h, stirring at room temperature. The samples were then dialyzed to remove unreacted FITC molecules, lyophilized and set at the concentration of 30µM in PBS (pH=7.4).

3.2.3 FITC conjugation quantification

FITC conjugation was confirmed using Varian Cary 50 Bio UV/Vis spectrophotometer. PBS served a baseline for the measurements. Fluorescence signal was quantified using a CLARIOstar Plus (BMG Labtech, Offenburg, Germany) microplate reader with settings for FITC (λ_{ex} 483-14 nm/ λ_{em} 530-30 nm). Briefly, each type of FITC-labelled nanoparticles was dissolved in methanol and diluted with PBS to the final concentration of 2 µg/ml. Standard curve was generated by preparing FITC standard solutions of 0.5 to 40ng/mL. Percent labelling efficiency was extracted as the proportion of FITC weight to the weight of PAMAM- (0%; 2%-350; 2%-5000) mPEG-FITC in the solution.

3.3 Transmission Electron Microscopy (TEM)

Nanoparticles were diluted to 15uM and the pH was adjusted to 6. Samples were briefly sonicated and a drop of dendrimeric nanoparticle suspension was placed on a 3mm holey carbon film coated copper grid (Ted Pella, Inc., Redding, California) and allowed to air-dry at room temperature. The samples were imaged using Orius CCD camera mounted on FEI Tecnai T20 transmission electron microscope. Average particle size analysis was performed using Image J. Data was fitted to log-normal distribution to obtain average size and standard deviation of the nanoparticles.

3.4 Dynamic Light Scattering (DLS)

30uM nanoparticle suspensions in PBS were assessed using Zetasizer Nano ZS system (Malvern Instruments, UK). Size of the nanoparticles was measured using disposable semi-micro UV-cuvettes (VWR, Leuven, Belgium), while for zeta potential measurements folded capillary zeta cells (DTS1070, Malvern, UK) were used. Hydrodynamic size and zeta potential is reported as a mean of three runs for each sample size (d.nm) ± s.d (d.nm) and PDI for each compound suspension was determined.

3.5 -Protein Corona isolation/formation

3.5.1 Patient-derived synovial fluid samples

All patients have provided informed consent and the procedure was approved by the Ethics Committee of Gothenburg University (Ethical approval Dnr: 573-07). Synovial fluid samples from 5 (4f/1m**)** RA patients and 4 **(**2f/2m**)** OA patients were collected during aseptic aspiration of knee joints at the Rheumatology Clinic and at the Orthopaedic Clinic respectively, Sahlgrenska University Hospital, Gothenburg, Sweden.

3.5.2 Protein Corona Formation

5 RA, 4 OA patient synovial fluid and control FBS samples were pooled according to the disease profile ($5x10^8$ particles or 2ug), diluted 1:20 in PBS and mixed with 30uM solution of PAMAM- (0%; 2%-350; 2%-5000) mPEG-FITC (1:1, v/v). The samples were incubated at 37°C while shaking for 1h. The particles were subsequently spun down at 15,000 x g for 15 minutes, washed twice with chilled PBS. The particles with adhered protein corona were resuspended to the final volume of 2 ml to a 1ug/ml ($2.5x10^8$ particles/mL) concentration in PBS and further processed according to below studies.

3.5.3 Proteomic Analysis

Nanoparticles with isolated protein coronas were pelleted, frozen using liquid nitrogen and submitted to the Proteomics Core Facility (Göteborg, Sweden). Briefly, proteins were digested into peptides using MS-grade trypsin and analyzed by nanoLC MS/MS. Mascot search engine was used to match the discovered peptide sequences against SwissProt protein database using Proteome Discoverer.

3.6 Cellular interactions with nanoparticles

Cellular studies focused on utilizing Tc28a2 chondrocyte cell line (a kind gift from Dr. Cronstein's lab at NYU Langone, USA) and cultured in DMEM, supplemented with 10% FBS and 1% GlutaMAX and grown at 5% CO2, relative humidity of 95%, and 37°C.

3.7 Cellular nanoparticle-corona uptake – flow cytometry

Cell medium was replaced to remove FBS as this could contribute to additional corona formation and thus was treated as one of the controls. The cells were seeded at $1x10^5$ cells/well in a 48-well plate. The cells were incubated with the particles at the indicated timepoints, washed three times in FACS buffer (1% FBS, 0,1 % NaN3 in 1xPBS) and analyzed by a Guava EasyCyte 8HT (Millipore, Darmstadt, Germany). Live cells were analyzed (after FSC/SSC exclusion of dead cells, >5000 cells) from within the gate were counted. The FITC was excited by a 488 nm laser, and fluorescence was detected through a 525/30 nm filter. The mean cellular uptake of FITC-labeled NP was estimated as the average fluorescence intensity of all cells within the gate. Each cell treatment was performed in three or four technical replicates (n = 3–4). All flow cytometry data was analyzed and visualized using FlowJo.

3.8 *Ex vivo* porcine-explant model of fluorescent nanoparticle uptake

Porcine tissue was obtained from the Experimental Biomedicine animal facilities under the 3R principle (Gothenburg, Sweden). The specimens entailed unexposed joints of the pig legs with femur and tibia still intact. Explants were frozen in PBS+PI+P/S (1%). When thawed or freshly introduced to culture, explants were allowed to equilibrate in the DMEM (without phenol red, supplemented with 25mM HEPES) overnight before the experiment.

To quantify FITC-labelled nanoparticle uptake into the cartilage, 4 mm puncher (Kai Medical, Honolulu, USA) biopsies were used to produce uniform explants of porcine cartilage with similar thickness to human. Explants were weighed to ensure uniformity before the experiments were started. Prior to nanoparticle administration, explants were placed in culture with 150µl DMEM lacking phenyl red, supplemented with 1% 10,000 U/mL Penicillin, Streptomycin (Gibco) and protease inhibitors (Roche, Switzerland) and allowed to equilibrate overnight. 100µl of 30µM PAMAM- (0%; 2%-350; 2%-5000) mPEG-FITC-protein corona nanoparticle solution was administered to the designated explants and incubated for 4 or 24 hours. The resultant FITC fluorescence in the supernatants and the explants was read at λ_{ex} 483-14 nm/ λ_{em} 530-30 nm using FITC settings on CLARIOstar Plus (BMG Labtech) as mentioned above. Each explant condition was performed in triplicates and repeated independently two-times. FITC amount was quantified using the FITC-based standard curve. Protein Quantification – BCA assay

3.10 Protein quantification

Protein content in the supernatant of the explants was assessed using a Pierce BCA protein assay kit according to manufacturer's instructions. Briefly, 10µl of the explant study supernatants were mixed with working reagent for 30 seconds and incubated for 30min at 37°C. Plate was allowed to cool to room temperature and the absorbance values at were measured at the wavelength of 562 nm. Standard curve of bovine serum albumin ranged from 2000µg/ml to 25 µg/ml. Every condition was investigated in three technical replicates.

3.11 sGAG quantification – DMMB assay

DMMB reagent was made by following the instructions of Kim, J. et al[15]. The standard stock solutions were prepared using chondroitin 4-sulfate sodium salt from bovine trachea (Sigma) with a detection window from 60ug/mL to 2.5 ug/mL. The result was obtained using a CLARIOstar Plus (BMG Labtech) microplate reader with the absorbance setting at 525 nm and the concentrations of sGAGs in the explant supernatant samples were elucidated from the standard curve. The studies were performed in triplicates for each sample condition.

3.12 Statistics

Data is presented as mean values ± SD unless otherwise indicated. Statistical analysis was performed using GraphPad Prism (GraphPad Software) version 9.0.2. One-way analysis of variance (ANOVA) was used to compare independent groups based on particle; all groups were statistically compared followed by Tukey's post hoc multiple comparisons test. P values <0.05 were considered statistically significant.

2.4 3.7 STATISTICS

Data is presented as mean values ± SD unless otherwise indicated. Statistical analysis was performed using GraphPad Prism (GraphPad Software) version 7.0b. T-test (comparing two groups) or one-way analysis of variance (ANOVA) was used to compare independent groups; all groups were statistically compared followed by Tukey's post hoc multiple comparisons test. P values <0.05 were considered statistically significant.

2.5 AUTHOR CONTRIBUTIONS

UvM and A.S designed the studies. UvM synthesized the polymers, conducted the in vitro and ex vivo studies and performed analysis. G.E conducted the NMR studies and analysis. L.R performed in vitro assays and analysis. A.K.H.E provided patient samples. UvM and A.S wrote the paper.

ACKNOWLEDGEMENTS

This work was supported by Chalmers Technical University, its Excellence Initiative Nano, and Area of Advance Health. The authors greatly acknowledge further financial support from the Kristina Stenborg foundation, the foundation for Sigurd and Elsa Goljes Minne, Apotekare Hedbergs Foundation, the King Gustav V's 80 years' foundation for founding.

COMPETING INTERESTS

The authors declare no competing interests.

REFERENCES

1. Glyn-Jones, S.; Palmer, A. J.; Agricola, R.; Price, A. J.; Vincent, T. L.; Weinans, H.; Carr, A. J., Osteoarthritis. *Lancet* **2015,** *386*, 376-87.
2. Bajpayee, A. G.; Grodzinsky, A. J., Cartilage-targeting drug delivery: can electrostatic interactions help? *Nat Rev Rheumatol* **2017,** *13*, 183-193.
3. Bajpayee, A. G.; Scheu, M.; Grodzinsky, A. J.; Porter, R. M., Electrostatic interactions enable rapid penetration, enhanced uptake and retention of intra-articular injected avidin in rat knee joints. *J Orthop Res* **2014,** *32*, 1044-51.
4. Lundqvist, M.; Cedervall, T., Three Decades of Research about the Corona Around Nanoparticles: Lessons Learned and Where to Go Now. *Small* **2020,** *16*, e2000892.
5. Garcia-Alvarez, R.; Hadjidemetriou, M.; Sanchez-Iglesias, A.; Liz-Marzan, L. M.; Kostarelos, K., In vivo formation of protein corona on gold nanoparticles. The effect of their size and shape. *Nanoscale* **2018,** *10*, 1256-1264.
6. Monopoli, M. P.; Aberg, C.; Salvati, A.; Dawson, K. A., Biomolecular coronas provide the biological identity of nanosized materials. *Nat Nanotechnol* **2012,** *7*, 779-86.
7. Walkey, C. D.; Chan, W. C., Understanding and controlling the interaction of nanomaterials with proteins in a physiological environment. *Chem Soc Rev* **2012,** *41*, 2780-99.
8. Madathiparambil Visalakshan, R.; Gonzalez Garcia, L. E.; Benzigar, M. R.; Ghazaryan, A.; Simon, J.; Mierczynska-Vasilev, A.; Michl, T. D.; Vinu, A.; Mailander, V.; Morsbach, S.; Landfester, K.; Vasilev, K., The Influence of Nanoparticle Shape on Protein Corona Formation. *Small* **2020,** *16*, e2000285.
9. Mirshafiee, V.; Kim, R.; Mahmoudi, M.; Kraft, M. L., The importance of selecting a proper biological milieu for protein corona analysis in vitro: Human plasma versus human serum. *Int J Biochem Cell Biol* **2016,** *75*, 188-95.
10. Kim, Y.; Klutz, A. M.; Jacobson, K. A., Systematic investigation of polyamidoamine dendrimers surface-modified with poly(ethylene glycol) for drug delivery applications: synthesis, characterization, and evaluation of cytotoxicity. *Bioconjug Chem* **2008,** *19*, 1660-72.

11. Schottler, S.; Becker, G.; Winzen, S.; Steinbach, T.; Mohr, K.; Landfester, K.; Mailander, V.; Wurm, F. R., Protein adsorption is required for stealth effect of poly(ethylene glycol)- and poly(phosphoester)-coated nanocarriers. *Nat Nanotechnol* **2016,** *11*, 372-7.
12. Harris, J. M.; Chess, R. B., Effect of pegylation on pharmaceuticals. *Nat Rev Drug Discov* **2003,** *2*, 214-21.
13. Ma, P.; Zhang, X.; Ni, L.; Li, J.; Zhang, F.; Wang, Z.; Lian, S.; Sun, K., Targeted delivery of polyamidoamine-paclitaxel conjugate functionalized with anti-human epidermal growth factor receptor 2 trastuzumab. *Int J Nanomedicine* **2015,** *10*, 2173-90.
14. Berrecoso, G.; Crecente-Campo, J.; Alonso, M. J., Unveiling the pitfalls of the protein corona of polymeric drug nanocarriers. *Drug Deliv Transl Res* **2020,** *10*, 730-750.
15. Kim, K. S.; Yoon, S. T.; Li, J.; Park, J. S.; Hutton, W. C., Disc degeneration in the rabbit: a biochemical and radiological comparison between four disc injury models. *Spine (Phila Pa 1976)* **2005,** *30*, 33-7.